ADVANCES IN INORGANIC CHEMISTRY AND RADIOCHEMISTRY, VOL. 21

A NEW LOOK AT STRUCTURE AND BONDING IN TRANSITION METAL COMPLEXES

JEREMY K. BURDETT*

Department of Inorganic Chemistry, The University, Newcastle upon Tyne, England

I. Introduction 113
II. Application of the Angular Overlap Method 114
A. Octahedral Transition Metal Ions 117
B. Tetrahedral Coordination 123
C. Other Geometries 124
D. Rates of Reaction of Hexaquo Ions 125
E. Geometries of Transition Metal Complexes 127
F. Derivation of Walsh Diagrams 134
G. Structural Consequences in d^8 and d^9 Systems 135
H. Ligand Site Preferences 138
I. Intramolecular Photochemical Rearrangements 141
III. Conclusion 143
References 143

I. Introduction

The construction of models of molecular geometry has been a popular exercise for many years. In the field of main-group stereochemistry the ideas of Sidgwick, Powell, Nyholm, and Gillespie have been successfully fused together into the VSEPR scheme (*1–3*), where the electron pairs around a central atom adopt the minimum energy consistent with their mutual electrostatic repulsion. The VSEPR rules have captured much of the essence of main-group stereochemistry and are unrivalled in their simplicity. In addition, Walsh diagrams (*4*) [quantified by the work of Gimarc and others (*5–8*)] and the pseudo Jahn–Teller formalism introduced by Bartell (*9*) into the structural field and extended by Pearson (*10*, *11*) have provided a molecular orbital interpretation of the wide range of available structural data.

By way of contrast, fewer gas-phase structures of transition metal complexes are known: a few d^0–d^4 hexafluorides (all octahedral), d^0–d^1 tetrachlorides (tetrahedral), and some 18-electron carbonyl and phosphine structures typified by tetrahedral $Ni(CO)_4$, octahedral

* Present address: Chemistry Department, University of Chicago, Chicago, Illinois 60637.

ISBN 0-12-023621-4

$Cr(CO)_6$, and trigonal bipyramidal $Fe(CO)_5$. Many transition metal systems are polymeric in the solid state yielding little or no data concerning their ideal "gas-phase" structure. Even when monomeric structures are established, we do not generally know how strong the influence is of crystal forces on the structure and geometry. This dearth of structural data has been alleviated considerably in recent years by the synthesis in low-temperature matrices of isolated carbonyl and dinitrogenyl fragments (*12*), $M(CO)_n$ and $M(N_2)_n$ ($n = 1$–6), with a variety of transition metal atoms M and, hence, a spectrum of d-orbital configurations that have filled some of the gaps in the structural field. Walsh diagrams have only recently been derived for transition metal complexes (*13*–*16*) but obviously need to be prolific in order to describe as completely as possible all possible distortion modes of ML_n ($n = 1$–6) systems. A simple model with a minimum of parameters would be a significant advance in the arena of structural transition metal chemistry. In this paper, we describe a molecular orbital parametrization that is able to provide a unified pathway to many structural problems.

II. Application of the Angular Overlap Method

Our simple molecular orbital approach is based on the angular overlap model (*17*), which has been used mostly in the past in the interpretation of the electronic spectra of transition metal complexes. Basically, it provides the energies of the (mainly) transition metal d orbitals in an ML_n complex of given geometry in terms of just two parameters [like the Δ or Dq of the crystal field theory (CFT)]. Once these energies have been derived then many structural effects may be examined, as we shall see in the following. For example, the weighted sum of these d-orbital energies (weighted by the number of electrons in these orbitals) as a function of the molecular geometry provides the opportunity to explore the configurational potential surface and, hence, find the minimum energy geometry demanded by the particular d-orbital configuration. The weighted sum of these energies relative to those of the free ion (the total d-orbital stabilization energy) leads to a rationalization of the heats of hydration of the transition metal ions. The relative stabilities of *cis*- and *trans*-ML_4L_2' octahedral complexes may be elucidated by considering the stabilization energies of each isomer. The angular overlap model, as we shall use it here, is based on an approximation involving the interaction energy between two orbitals ϕ_i, ϕ_j on different atoms. In our case ϕ_i will represent a d orbital on the transition metal center, and ϕ_j a single-ligand orbital or

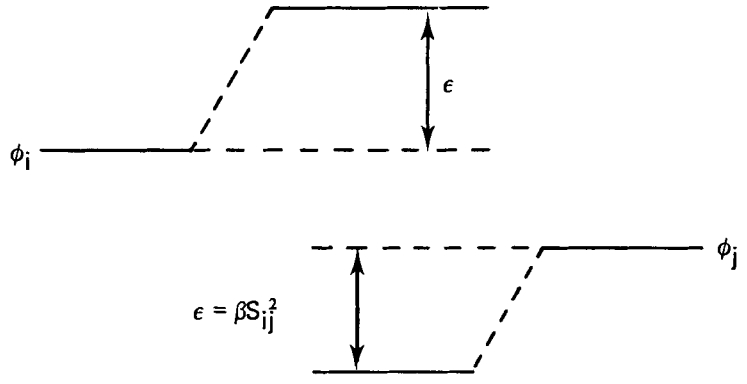

FIG. 1. Energy-level diagram showing the basis of the model. Stabilization of bonding orbital = destabilization of antibonding orbital = βS_{ij}^2.

a symmetry-adapted combination of ligand orbitals transforming under the same irreducible representation as ϕ_i.

The angular overlap approximation sets the stabilization energy of the bonding orbital proportional to the square of the overlap integral between ϕ_i and ϕ_j, $\epsilon = \beta S_{ij}^2$, where β is a constant inversely dependent on the energy separation between ϕ_i and ϕ_j. In our simple model, we shall assume in addition that the destabilization energy of the antibonding orbital is equal to this stabilization energy of the bonding orbital[1] (Fig. 1). The tremendous power of the model lies in the fact that the S_{ij} are, in general, dependent on simple geometric expressions as the angular metal–ligand geometry is adjusted while maintaining the same bond length. Figure 2 shows pictorially the simple function describing the overlap integral between a central atom p_z orbital and ligand σ orbital in terms of the polar coordinate θ. S_σ is a constant[2] and equal to the overlap integral between the two orbitals for $\theta = 0$.

[1] This is not strictly true (*17e*):

$$\Delta\epsilon_{anti} = \frac{H_{LL}^2}{H_{MM} - H_{LL}} S_{ML}^2$$

and

$$\Delta\epsilon_{bond} = \frac{H_{MM}^2}{H_{MM} - H_{LL}} S_{ML}^2$$

i.e., the antibonding orbital receives a larger destabilization than the stabilization received by the bonding orbital. Inclusion of overlap between ϕ_i and ϕ_j will also tend to push both new orbitals to higher energy and increase the disparity. (H_{LL} and H_{MM} are the ionization potentials of ligand and metal orbitals, respectively.)

[2] The notation we have chosen to use here is that of Kettle (*17f*).

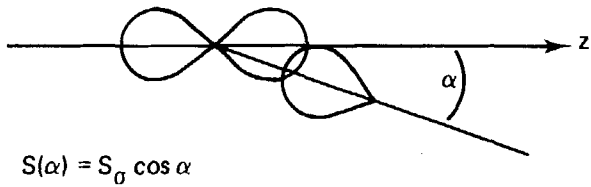

FIG. 2. Overlap of a ligand σ orbital with a central atom p orbital as a function of angle.

TABLE I

OVERLAP INTEGRALS OF CENTRAL ATOM d ORBITALS AS A FUNCTION OF THE LIGAND POSITION IN POLAR COORDINATES (θ, ϕ) WITH A LIGAND σ ORBITAL[a,b]

d_{z^2}	$\frac{1}{2}(3\cos^2\theta - 1)S_\sigma$[c]
$d_{x^2-y^2}$	$(\sqrt{3}/2)\cos^2\phi \sin^2\theta\, S_\sigma$
d_{xz}	$(\sqrt{3}/2)\cos\phi \sin^2\theta\, S_\sigma$
d_{yz}	$(\sqrt{3}/2)\sin\phi \sin^2\theta\, S_\sigma$
d_{xy}	$(\sqrt{3}/2)\sin^2\phi \sin^2\theta\, S_\sigma$

[a] For simplicity, π-type overlap functions have been left off this table. Their values are given in Larsen and La Mar (*17g*).

[b] See Fig. 3, regarding labeling of polar coordinates and ligand.

[c] S_σ Is the overlap of a ligand σ orbital with d_{z^2} when the ligand lies along the z axis.

For the two orbitals of Fig. 2, the interaction energy as a function of angle is thus simply $\epsilon = \beta_\sigma S_\sigma^2 \cos^2\theta$, here we introduce β_σ as the β parameter describing interactions that are of σ type.[3] For interactions between orbitals of π type, we introduce two similar parameters β_π and S_π. Table I gives the angular dependence of the overlap integrals between the d orbitals and ligand σ-type orbitals; the ligand position is defined by the polar angles θ, ϕ. Also π-type interactions are amenable to similar treatment.[4]

We are thus in a position to be able to write the interaction energy of a pair of orbitals as a simple expression $\epsilon = kf(\theta, \phi)$, where k is a constant, and $f(\theta, \phi)$ a simple geometric function readily obtained from

[3] An interesting forerunner of the angular overlap model is given by McClure (*19*).

[4] The integrals involving s, p, and f orbitals are available in Smith and Clack (*20*).

Table I. This is the basis of our approach and is really quite a simple one to use, although obviously not as simple as the VSEPR rules (*18*) in main-group stereochemistry.

A. Octahedral Transition Metal Ions

The octahedrally coordinated molecule provides a useful introduction to the practicalities of the method. The ligand σ orbitals transform as $a_{1g} + e_g + t_{1u}$, the ligand π orbitals as $t_{1g} + t_{2g} + t_{1u} + t_{2u}$, and the metal d orbitals as e_g and t_{2g}. We are interested, therefore, in the σ interactions (of species e_g) and the π interactions of (species t_{2g}) of the ligand orbitals with the metal.

1. σ-Type Interactions

For one component of the doubly degenerate, e_g ligand combination, we may write

$$\psi_{e_g}(1) = \tfrac{1}{2}(\phi_1 - \phi_2 + \phi_3 - \phi_4) \tag{1}$$

with reference to Fig. 3. The overlap integral functions contained in Table I allow us to calculate the relevant overlap integral between

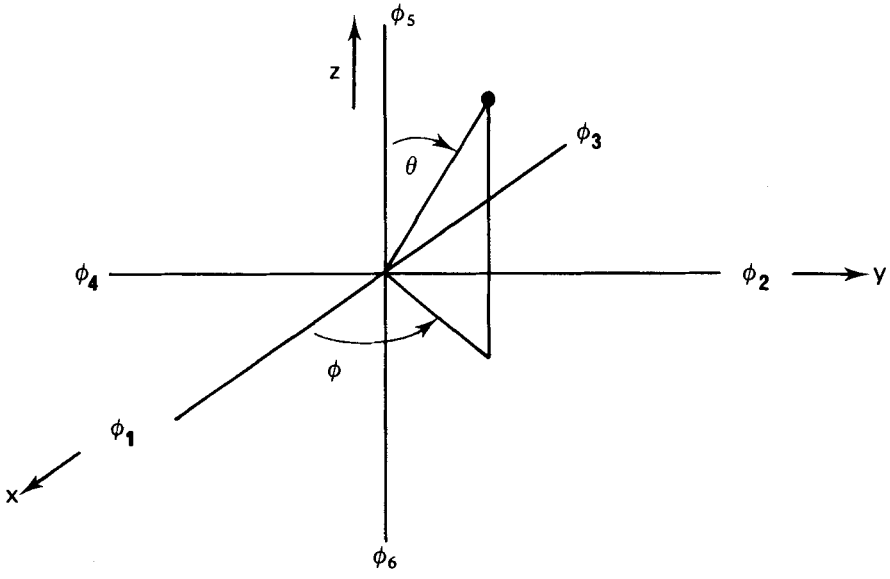

FIG. 3. Polar coordinates and ligand σ-orbital labeling in the octahedron.

$\psi_{e_g}(1)$ and $d_{x^2-y^2}$. In Table I, with reference to Fig. 3, $\theta = 90°$ and $\phi = 0°, 90°, 180°, 270°$ for the overlap integrals involving $\phi_1 \rightarrow \phi_4$. Thus we immediately find

$$S_{e_g}(1) = 1/2 \cdot 4 \frac{\sqrt{3}}{2} S_\sigma \tag{2}$$

i.e., $\epsilon(e_g) = 3\beta_\sigma S_\sigma^2$. For the octahedral geometry (and other octahedrally based structures such as the square plane), we will find Table II useful. This gives the overlap integrals of a ligand σ orbital located along x, y, or z axes with $d_{x^2-y^2}$ and d_{z^2}, and is simply a rationalized form of a part of Table I.

TABLE II

OVERLAP INTEGRALS OF A LIGAND σ ORBITAL WITH d_{z^2} AND $d_{x^2-y^2}$

	Ligand located along	
Overlap integral with	x, y	z
d_{z^2}	$-\frac{1}{2} S_\sigma$	S_σ
$d_{x^2-y^2}$	$\pm(\sqrt{3}/2)S_\sigma$	0

We may similarly construct a ligand e_g σ-orbital combination to overlap with d_{z^2},

$$\psi_{e_g}(2) = \frac{1}{\sqrt{12}}(2\phi_5 + 2\phi_6 - \phi_1 - \phi_2 - \phi_3 - \phi_4) \tag{3}$$

and, by using Table II, we find

$$S_{e_g}(2) = \frac{1}{\sqrt{12}}(2 + 2 + \tfrac{1}{2} + \tfrac{1}{2} + \tfrac{1}{2} + \tfrac{1}{2})S_\sigma = \frac{6}{\sqrt{12}} S_\sigma \tag{4}$$

Hence the stabilization energy is $3\beta_\sigma S_\sigma^2$ as it has to be by symmetry with Eqs. (1) and (2). Figure 4 shows the molecular orbital diagram for the σ framework of the octahedral configuration using this result and our aforementioned assumption concerning stabilization in bonding and antibonding orbitals. Also shown is the well-known crystal field-splitting pattern for this geometry. We see immediately that $\Delta_{oct} = 3\beta_\sigma S_\sigma^2$.

We are now in a position to calculate the total stabilization energy of an ML_6 complex from the free ion plus ligands (*21*). We shall compare

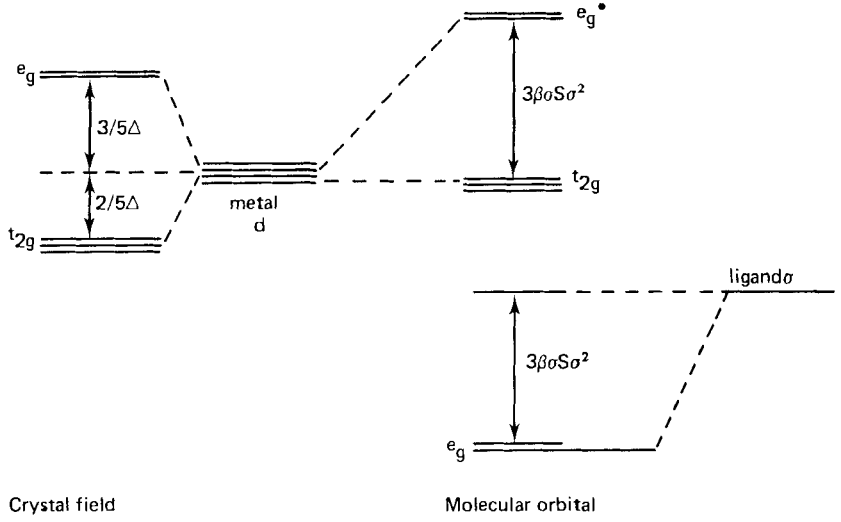

FIG. 4. Comparison of crystal field and molecular orbital methods for the octahedral environment.

the result with the familiar "double-humped" curve (*22, 23*) associated with ΔH^0_{hyd} for the reaction

$$M^{2+}\ (gas) + 6H_2O\ (gas) \rightarrow M^{+2}(H_2O)_6\ (gas) \tag{5}$$

For all d^n complexes the e_g bonding orbitals (mainly ligand located) contain 4 electrons and these contribute (from Fig. 4) a stabilization energy of $4 \times 3\beta_\sigma S_\sigma^2 = 12\beta_\sigma S_\sigma^2$. The first 3 d electrons experience no change in energy on complex formation—they go into σ nonbonding d orbitals and, thus, $\sum(\sigma) = 12\beta_\sigma S_\sigma^2$, where we introduce symbol $\sum(\sigma)$ to describe the total σ-stabilization energy of a given electronic configuration. The fourth electron of the high-spin d^4 complex, however, enters e_g^* and is destabilized by $3\beta_\sigma S_\sigma^2$. The total σ-stabilization energy $\sum(\sigma)$ is thus equal now to only $9\beta_\sigma S_\sigma^2$. We may readily calculate the values of $\sum(\sigma)$ for all the high-spin configurations d^0-d^{10}, and these are plotted in Fig. 5. An equation we shall find useful later on in evaluating these $\sum(\sigma)$ values is

$$\sum(\sigma) = \sum_i h_i \beta_\sigma S_i^2 \tag{6}$$

where $\beta_\sigma S_i^2$ is the interaction energy of the ith d orbital, and h_i is the number of electron holes in this orbital. Equation (6) (*24*) arises simply

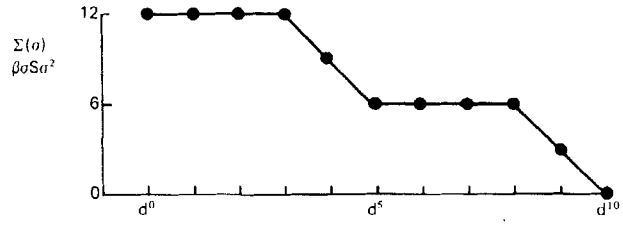

FIG. 5. Plot of d-Orbital σ-stabilization energies [$\sum(\sigma)$] for high-spin d^n ions.

because when filling d orbitals with electrons we are filling metal–ligand *anti*bonding orbitals, and it is only the *empty* d orbitals that have filled metal–ligand bonding counterparts which contribute to the stabilization energy.

This plot of Fig. 5 is not immediately recognizable as being associated with the familiar double-humped curve describing ΔH^0_{hyd} as a function of the number of d electrons. However, we should recall that in addition to interaction with the metal *n*d orbitals, the ligands are attached to the transition metal ion by interactions with the $(n + 1)$s and $(n + 1)$p orbitals. How else would the $Zn(H_2O)_6^{2+}$ (d^{10}) complex be stabilized with all metal d-ligand antibonding orbitals occupied? Thus, the observed ΔH^0_{hyd} plot will be the sum of these s + p orbital stabilization energies and the d-orbital contribution[5] of Fig. 5.

Figure 6a shows how a sloping (s + p) contribution can be added to the d-orbital function of Fig. 5 to give the observed variation along the series. Figure 6b shows the crystal field rationalization of the effect in terms of the crystal field stabilization energy. The slope of the s + p contribution of Fig. 6a is readily rationalized. As the first-row transition metal series is traversed, the ionization potential of the metal becomes larger and shifts the entire set of s + p + d orbitals to lower energy. The s, p energy separation from the ligand σ orbitals thus decreases across the series and, correspondingly, the stabilization energy increases. This molecular orbital rationalization of the data in Fig. 6 is certainly more convincing than previous molecular orbital explanations (*23*). We have in addition produced with the minimum of effort the relative contributions of d and higher orbitals to the total stabilization energy associated with metal–ligand (in this case H_2O)

[5] Because we are dealing with high-spin systems, the same combination of electron repulsion terms as for the lowest-energy term of the gaseous ion will occur, in the form of the Racah parameters, in the energy description of the ground electronic state of the complex. Thus, we are perfectly justified in only considering the change in orbital energy on complex formation.

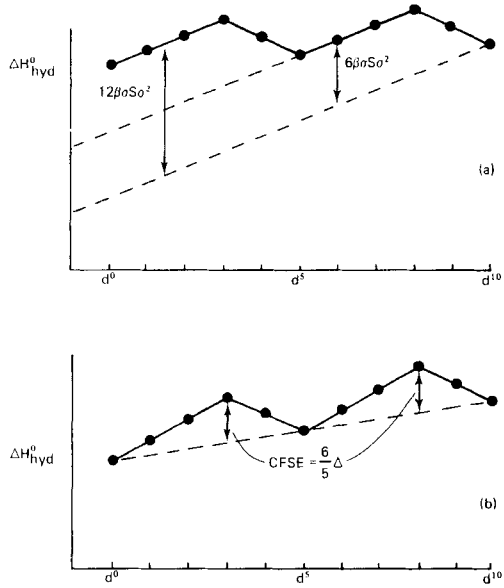

FIG. 6. Molecular orbital (a) and crystal field (b) rationalizations of the variation of ΔH^0_{hyd} with d^n.

interaction. For Ti^{2+}, the d-orbital contribution is about 50% but for Cu^{2+}, only about 15%. We must, therefore, exercise considerable care in the interpretation of structural transition metal data in d-orbital terms alone—higher orbital contributions are obviously very important in numerical terms. Having said this, we shall be surprised to find that a large amount of material can be rationalized using the d-orbital-only model.

The actual mixing of *n*d and $(n + 1)$p orbitals is, of course, of crucial importance in providing a mechanism by which the Laporte forbidden d-d transitions in transition metal complexes may gain in intensity. This may occur in the static situation (e.g., tetrahedral complexes), where the p orbitals and one set of the d orbitals transform as t_2 or in the dynamic situation (as in octahedral complexes) where such mixing is only possible when the point symmetry has been reduced by an asymmetric vibration (vibronic coupling).

2. *π-Bonding*

The π-bonding may be treated along exactly the same lines as just shown for σ-type interactions. No new principles are needed. Structure

I shows one component of the ligand t_{2g} combination, and we may

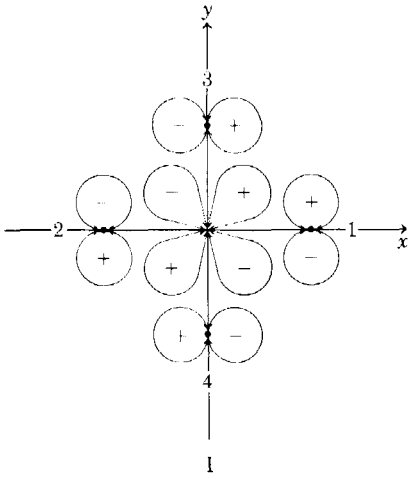

write

$$\psi_{t_{2g}}(1) = \tfrac{1}{2}(\pi_3 - \pi_4 + \pi_5 - \pi_6) \tag{7}$$

If the overlap of one lobe of d_{xy} with a ligand π-type orbital along the x axis is defined as S_π, the overlap of Eq. (7) with d_{xy} becomes

$$S_{t_{2g}}(1) = \tfrac{1}{2} \cdot 4 \cdot S_\pi \tag{8}$$

and, thus, the π-interaction energy $\epsilon = 4\beta_\pi S_\pi^2$. For systems containing π donors (where the ligand π orbitals lie below the d orbitals), the t_{2g} d-orbital set is raised in energy by this amount; with π acceptors (where the ligand π orbitals lie above the d orbitals), the t_{2g} d orbitals are depressed by $4\beta_\pi S_\pi^2$. The crystal field-splitting parameter Δ is then related to the angular overlap parameters by $\Delta_{oct} = 3\beta_\sigma S_\sigma^2 \pm 4\beta_\pi S_\pi^2$, the choice of sign depending on the nature of the π orbitals present. The interaction energy involving the ith d orbital may also be derived using

$$\epsilon_i = \beta \sum_j S_{ij}^2 \tag{9}$$

where the summation is over all ligand orbtials j. In the present case we have four ligand orbtials each having an overlap integral of S_π with d_{xy} and thus $\epsilon(d_{xy}) = 4 \times \beta_\pi S_\pi^2$ as before. Use of Eq. (9) gives the same results as for the σ-type interactions in the foregoing, and it is very easy quickly to derive orbital energies using this equation and Tables I and II without recourse to group theory.

B. Tetrahedral Coordination

By the same methods as discribed in Section II, A, we may construct t_2 functions of σ symmetry with which to overlap with the d_{xz}, d_{xy}, and d_{yz} orbitals in the tetrahedral configuration. The interaction energy becomes $\epsilon(t_2) = 1.333\ \beta_\sigma S_\sigma^2$ for this geometry. Inclusion of π bonding leads to the energy levels of Fig. 7 for π donors. (For π acceptors, the π contribution is included with the opposite sign.) Immediately we notice that, whereas $\Delta_{oct} = 3\beta_\sigma S_\sigma^2 \pm 4\beta_\pi S_\pi^2$, $\Delta_{tet} = (4/3)\beta_\sigma S_\sigma^2 \pm (16/9)\beta_\pi S_\pi^2$, i.e., $\Delta_{tet} = (4/9)\Delta_{oct}$. (The equality will only hold, of course, if $\beta_\sigma S_\sigma$ is the same in both geometries, i.e., the metal–ligand distance remains constant.) One rule that we will find useful in the derivation of these figures is a sum rule concerning the orbital energies (*17c*).

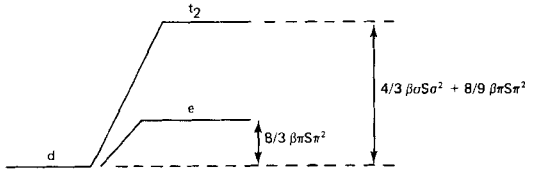

Fig. 7. Energy-level diagram for tetrahedral coordination of a σ and π donor (π contributions should be included with opposite sign for π acceptors).

In a complex ML_n, where there are $n\sigma$ orbitals directed at the central atom the sum total σ interaction energy of all the d orbitals is simply equal to $n\beta_\sigma S_\sigma^2$. Thus we know in the octahedral case that all the σ interaction is contained in the doubly degenerate e_g set of orbitals from group theory. The total available σ interaction energy ($6\beta_\sigma S_\sigma^2$) is, therefore, shared between each of the two components of the e_g set, i.e., $3\beta_\sigma S_\sigma^2$ each. In the tetrahedral molecule the total σ interaction energy ($4\beta_\sigma S_\sigma^2$) is shared between the three components of the t_2 set, i.e., $(4/3)\beta_\sigma S_\sigma^2$ each. Similarly, if each ligand has two orbitals of π symmetry the total π interaction is $2n\beta_\pi S_\pi^2$. In the octahedral case the total π interaction, $12\beta_\pi S_\pi^2$, is shared between the three components of the t_{2g} set of orbitals, $4\beta_\pi S_\pi^2$ each. In the tetrahedron, both t_2 and e sets contain π contributions, and the total interaction energy of $8\beta_\pi S_\pi^2$ is shared between the two. To calculate what fraction is located in the t_2 set and what function in the e set, we need to write down a symmetry-adapted ligand wavefunction and calculate the overlap integral as we have shown previously. However, since the sum total is $8\beta_\pi S_\pi^2$, once the π contribution to one set has been decided by this calculation, the contribution to the other set can obviously be obtained by simple subtraction. The combination of this sum rule and Eq. (9)

allows a rapid calculation of the d-orbital energies for different geometries.

C. Other Geometries

Energy-level diagrams for other geometries are now readily derived. Because inorganic chemists place greater stress on σ interactions than on π interactions, we shall emphasize the former in what follows and initially ignore the π contributions to the orbital energies. By using Eq. (9) and Table II, we can readily derive the interaction energies associated with the $d_{x^2-y^2}$ and d_{z^2} orbitals in the orthogonal geometries derived from the octahedron. For example in the square planar structure (II), the four σ ligands overlap with $d_{x^2-y^2}$ to give a total interaction energy of $4 \times \beta_\sigma(\sqrt{3}/2)^2 S_\sigma{}^2 = 3\beta_\sigma S_\sigma{}^2$ and with the "collar" of d_{z^2} to give a total interaction energy of $4 \times \beta_\sigma(1/2)^2 S_\sigma{}^2 = \beta_\sigma S_\sigma{}^2$. Figure 8 shows d-orbital energy-level diagrams for some of these octahedrally based geometries and the trigonal plane and trigonal bipyramid.[6] We

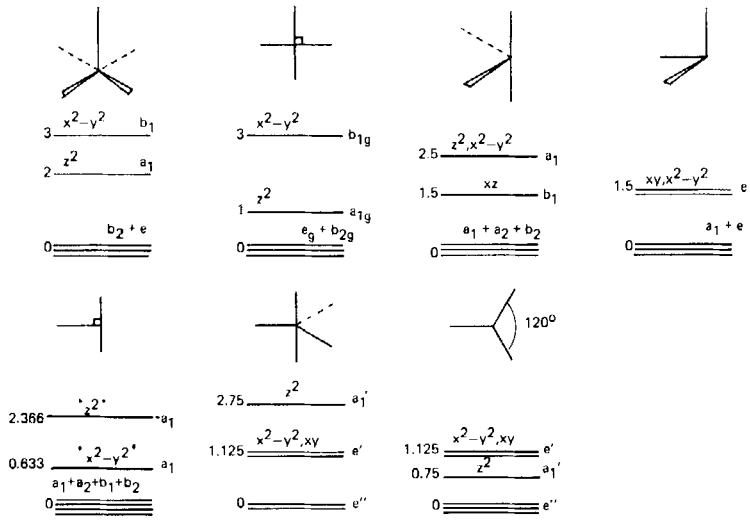

FIG. 8. Energy-level diagrams for some geometries of interest.

[6] In the low-symmetry situation of the T-shaped structure, orbitals d_{z^2} and $d_{x^2-y^2}$ must always mix together. (In the cis-divacant structure this is avoided by a suitable choice of axes.) Solution of the relevant determinant gives us $\epsilon = (1.5 \pm \sqrt{3})\beta_\sigma S_\sigma{}^2$ for the two interacting orbitals [see McClure (*19*) for a more complete discussion]. In Burdett (*24*) such mixing was ignored.

remember that to lower energy, the ligand σ orbitals split apart in energy as the mirror image of this d-orbital splitting. However, we need only the d-orbital region of the energy-level diagram to calculate the total d-orbital stabilization energy of a given electronic configuration since $\sum(\sigma)$ of Eq. (6) depends only on the location of the holes in the d-orbital manifold.

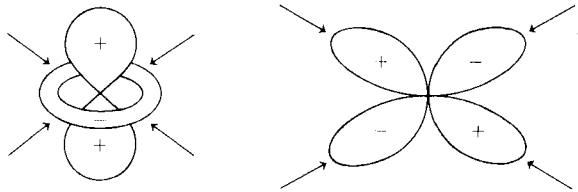

II

D. Rates of Reaction of Hexaquo Ions

Knowledge of the energy-level diagram for the square pyramidal geometry allows us to rationalize immediately (*22*) the rates of ligand labilization in $M(H_2O)_6^{2+}$ molecules (k_1), determined in the classical

$$\underset{\text{octahedral}}{M(H_2O)_6^{2+}} \overset{k_1}{=} \underset{\text{square pyramidal}}{M(H_2O)_5^{2+}} + H_2O$$

researches of Eigen (*25*, *26*). Simple subtraction of the d-orbital stabilization energies for octahedral and square pyramidal molecules gives the contribution of the metal d orbitals to the energy of activation for ligand loss shown in Fig. 9 as a function of the number of d electrons (all electronic configurations and high-spin). This is simply done by use of Eq. (6) and the relevant energy-level diagrams of Figs. 4 and 8. If a sloping contribution from s + p orbital interactions is added (cf. the heats of hydration themselves in Fig. 6a), then the curve of Fig.

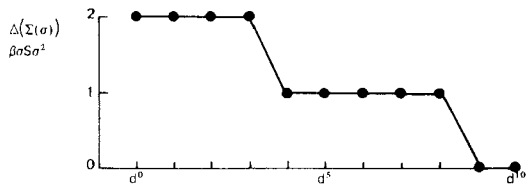

FIG. 9. Difference in d-orbital σ-stabilization energies [$\Delta(\sum(\sigma))$] between octahedral and square pyramidal d^n ions.

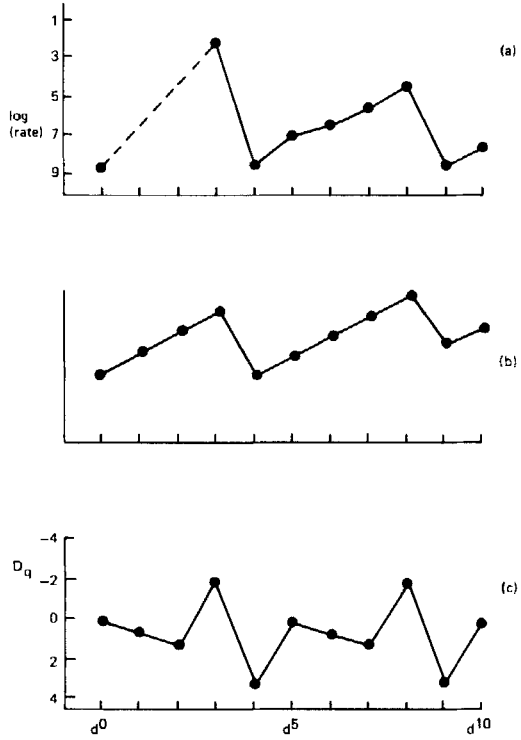

FIG. 10. Molecular orbital rationalization of the rates of reaction of hexaquo ions: (a) experiment; (b) theory; and (c) crystal field approach.

10b results. This is to be compared with the observed rates (Fig. 10a) and the crystal field analysis of the activation energy (Fig. 10c) obtained by simple subtraction of the CFSE's of octahedron and square pyramid.[7]

The superiority of the molecular orbital approach is clear; the activation energy is always positive which is not the case with the CFT, and the molecular orbital plot is quite a faithful reproduction of the observed log (rate) curve. The failure of the CFT is due to the following reason. In the absence of π bonding, Fig. 8 shows that the lowest three d orbitals are equienergetic (b_2 + e) for the square-based pyramid, but the nature of the CF method removes this accidental degeneracy considerably. In terms of Dq, the CF energies of the d

[7] For a discussion of the crystal field rationalization of this data, see Philipps and Williams (*27*).

orbitals in the square pyramid are

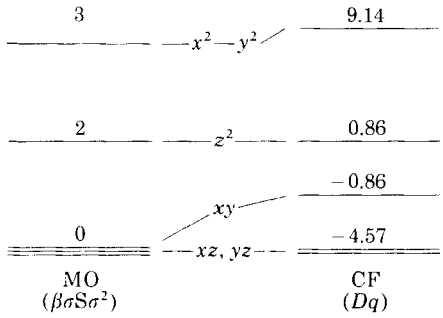

It is the large splitting between d_{xy} and d_{xz}, d_{yz}, not reproducible on a no π-bonding molecular orbital model, which gives rise to the incorrect form of the plot of Fig. 10c. The error in the CFT will, of course, be especially apparent in those systems which are poor π bonders as is the present case with the aquo ligand. In general, then, the CFT should not be trusted to give a quantitative measure of the d-orbital splittings.

E. Geometries of Transition Metal Complexes

We have seen in Section II,D the relative contributions of the metal s and p orbitals compared to d orbitals to the heats of hydration and rates of reaction of the hexaquo ions. In the field of molecular geometry, these observations suggest that here the geometry will be a compromise between that demanded by the s,p-orbital interactions and that by the d-orbital interactions with the ligands. In general, an ML_n complex will contain $n\sigma$ pairs of electrons involved in s,p (and d) interactions. Thus, on the basis of the VSEPR method (dealing exclusively with molecules involving s,p orbitals on the central atom), the geometry demanded by interactions with these higher orbitals will be (*3*): trigonal planar (D_{3h}) for ML_3, tetrahedral (T_d) for ML_4, trigonal bipyramidal (D_{3h}) for ML_5 and octahedral (O_h) for ML_6. We note that the VSEPR geometry in these cases is the one with minimum ligand-pair repulsions [Pauli avoidance (*18*)] and also the geometry containing minimum nonbonded repulsions between the ligands themselves. We will label these combined forces ligand-ligand terms. The geometries of some four-coordinate $M(CX)_4$ species with different d^n configurations, shown in Fig. 11, indicate that the d orbitals may often exert a decisive effect in modifying this VSEPR geometry.

Let us start by looking at these four-coordinate geometries. The σ stabilization energy, $\sum(\sigma)$, derived using Eq. (6) and the energy-level

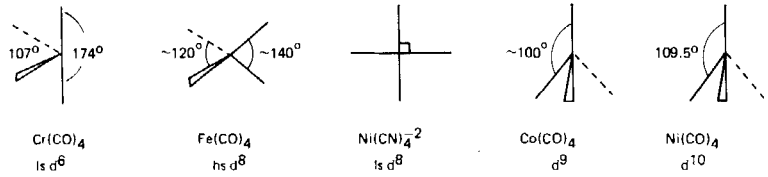

FIG. 11. Some four-coordinate geometries (ls, low-spin; hs, high-spin).

diagrams of Fig. 8, allow ready construction of Table III for three geometries of interest, namely, the octahedral "cis-divacant" (or butterfly or disphenoidal) structure, the square plane, and the tetrahedron. For the d^{10} configuration we see that no d-orbital stabilization energy is present since all metal (d)–ligand σ-bonding and antibonding orbitals are equally occupied. The tetrahedral structure of $Ni(CO)_4$ or $ZnCl_4^{-2}$ thus results, since this is the geometry demanded by ligand-ligand interactions of the type described in the foregoing. For the d^9, low-spin d^8 and d^7 systems, the square planar geometry has the largest d-orbital stabilization energy. For the low-spin d^8 system, the square planar geometry is more favored (by $3.33\beta_\sigma S_\sigma^2$) relative to the tetrahedral (the ligand-ligand determined geometry). Low-spin d^8 systems are always square planar e.g., $Ni(CN)_4^{-2}$. The square planar geometry is similarly strongly favored for the low-spin d^7 configuration (by $3\beta_\sigma S_\sigma^2$) and all low-spin Co(II) systems are square planar.

For the d^9 configuration, square planar is still favored relative to tetrahedral but by a smaller amount ($1.66\beta_\sigma S_\sigma^2$). For Cu(II) complexes with this configuration, the geometry often depends on the crystal structure and the nature of the counterion. For example, $(NH_4)_2CuCl_4$ contains (*28a*) planar $CuCl_4^{-2}$ ions, but Cs_2CuCl_4 and Cs_2CuBr_4 and, in general, systems with large cations contain CuX_4^{-2} ions that are

TABLE III

TOTAL d-ORBITAL STABILIZATION ENERGIES [$\sum(\sigma)$] FOR FOUR-COORDINATE COMPLEXES (UNITS $\beta_\sigma S_\sigma^2$)

Configuration[a]	cis-Divacant	Square planar	Tetrahedral
d^{10}	0	0	0
d^9	2.5	3	1.33
d^8(ls)	5	6	2.67
d^8(hs)	4	4	2.67
d^7(ls)	6.5	7	4
d^6(ls)	8	8	5.67

[a] Low spin (ls); high spin (hs).

squashed tetrahedra (*28b*) of the D_{2d} point group (III), i.e., halfway between the ligand-ligand (tetrahedral) and d-orbital (square planar) structures. The two geometries are close in energy for this electronic configuration, as evidenced by the fact that application of pressure (*29*) sends the squashed tetrahedron in Cs_2CuBr_4, Cs_2CuCl_4, or $[(CH_3)_2CHNH_3]_2\,CuCl_4$ to the square planar geometry.

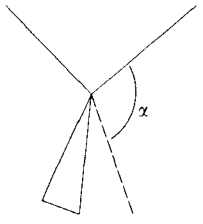

III

The process is reversible.[8] The d-orbital stabilization energy is, therefore, often only large enough to drive the structure a part of the way toward the square planar geometry. Two independent, molecular orbital calculations (*13*, *15*) for a d^9 tetracarbonyl moiety predict angles α of 132° and 135° for the equilibrium geometry, i.e., halfway between tetrahedral (110°) and square planar (180°). In fact for $Co(CO)_4$ both D_{2d} and C_{3v} (angle C_{ax}-M-$C_{eq} \simeq 100°$) structures are found (*31*) for this species, trapped in a low-temperature matrix. For small distortions away from tetrahedral, there is not much to choose between these two structures for the d^9 configuration.

For two electronic configurations of Table III the square planar and cis-divacant structures are predicted to be of equal stability. In order to determine the one of lowest energy, it is necessary to extend the angular overlap approximation to the fourth power in the overlap integral S. The general result (*24*) is that the more stable structure is the one with the larger number of cis ligands—in this case, the cis-divacant structure. The fact that we need to resort to terms in S^4 means that the energy differences between the various geometries is smaller for these (e.g., low-spin d^6) systems than for low-spin d^7. We will see some consequences of this later in the stability of cis and trans octahedral isomers ML_4L_2'. The cis-divacant geometry is that observed for (*32*) matrix-isolated $Cr(CO)_4$ (Fig. 11), where the energy difference

[8] Ferraro and Long (*30*) have used the second-order Jahn–Teller formalism to give some clues as to why these ions should distort along this pathway linking the tetrahedron and square plane. The present author has suggested (*24*) that this is only valid for systems containing a single d-orbital hole (as in these d^9 systems), but this is not a completely general approach.

from tetrahedral is $2.33\beta_\sigma S_\sigma^2$. For high-spin d^8, however, the d-orbital stabilization energy difference between the two geometries is smaller ($1.33\beta_\sigma S_\sigma^2$). For the four-coordinate d^9 system with a difference of $1.66\beta_\sigma S_\sigma^2$, we found geometries intermediate between the tetrahedron and the geometry demanded on d-orbital grounds alone. Similarly high-spin d^8 systems are usually described as distorted tetrahedral and are typified by the matrix-isolated $Fe(CO)_4$ structure (*33*) of Fig. 11. They are, therefore, intermediate in structure between the tetrahedral and cis-divacant arrangements.

For five-coordinate molecules, we find the stabilization energies (Table IV) for five electronic configurations of interest. For low-spin d^6, the stabilization energy difference between the square pyramid and the trigonal bipyramid (the ligand-ligand determined geometry) is largest and matrix-isolated $M(CO)_5$ (M = Cr, Mo, W) is found to have the C_{4v} geometry (*34*). Preliminary reports point to square pyramidal geometries for $Re(CO)_5$ (*35*) and $Mn(CO)_5$ (*36*). Ab initio molecular orbital calculations conclude a square pyramidal structure (*37*). However, for d^6 (intermediate spin) and low-spin d^8, the energy difference between the two geometries is very small. The species $Fe(CO)_5$ is well known in the gas phase as a trigonal bipyramidal molecule (*38*) [as is the $Mn(CO)_5^-$ in the crystal (*39*)], although the molecule is fluxional and rapidly exchanges axial and equatorial sites probably via the square pyramidal configuration [Berry process (*40*)] as intermediate. The ion $Ni(CN)_5^{-2}$ exists in the crystal as a mixture of trigonal bipyramidal and square pyramidal molecules, but application of pressure (*41*) reversibly sends all the molecules into the square pyramidal structure at 7 kbar. The photochemistry of $Cr(CO)_5$ and $Mo(CO)_4 - Pcy_3$ (low-spin d^6) may be explained (*42*) on the basis that

TABLE IV

TOTAL d-ORBITAL STABILIZATION ENERGIES [$\sum(\sigma)$] FOR SOME FIVE-COORDINATE COMPLEXES (UNITS $\beta_\sigma S_\sigma^2$)

Configuration[a]	Square pyramid	Trigonal bipyramid	Difference
d^9	3	2.75	0.25
d^8(ls)	6	5.5	0.5
d^7(ls)	8	6.625	1.375
d^6(ls)	10	7.75[b]	2.25
d^6(ls)	8	7.75[b]	0.25

[a] Low spin (ls).

[b] These two electronic configurations have identical d-orbital electronic distributions in the trigonal bipyramidal geometry.

TABLE V

TOTAL d-ORBITAL STABILIZATION ENERGIES [$\sum(\sigma)$] FOR SOME THREE-COORDINATE COMPLEXES (UNITS $\beta_\sigma S_\sigma^2$)

Configuration[a]	Trigonal plane	T shape	C_{3v}[b]
d^{10}	0	0	0
d^9	1.125	2.366	1.5
d^8(hs)	2.25	3	3
d^8(ls)	2.25	4.732	3
d^7(ls)	3.375	5.366	4.5
d^6(ls)	4.5	6	6

[a] High spin (hs); low spin (ls).
[b] All bond angles 90°.

the first electronic excited state (intermediate-spin d^6) has a trigonal bipyramidal geometry. We return to this point later.

For three-coordinate molecules we derive the stabilization energies shown in Table V. To distinguish between the equienergetic geometries for high-spin d^8 and low-spin d^6 systems, we use the rule already developed here that the most stable geometry is the arrangement with the maximum number of cis ligands. Experimentally the d^{10} species $Ni(CO)_3$, $Ni(N_2)_3$, etc. (*43*) are found from matrix isolation studies to be trigonal planar (D_{3h}). The structure of $Cr(CO)_3$ (low-spin d^6) closely resembles (*32*) the C_{3v} structure with orthogonal ligands (IV). Here the difference in stabilization energy between C_{3v} and D_{3h} is $1.5\beta_\sigma S_\sigma^2$.

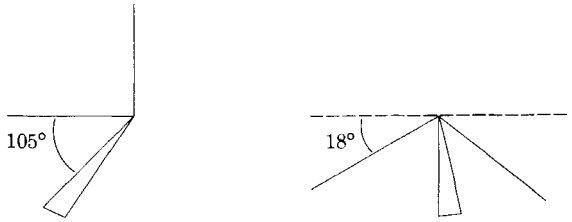

IV

For high-spin d^8, the stabilization energy is smaller ($0.75\beta_\sigma S_\sigma^2$) and a structure halfway between the d-orbital, and ligand-ligand determined geometries is found (*44*) for $Fe(CO)_3$. Perhaps this smaller energy difference between C_{3v} and D_{3h} $Cr(CO)_3$ molecules ($1.5\beta_\sigma S_\sigma^2$) than between the C_{2v} and T_d $Cr(CO)_4$ molecules ($2.33\beta_\sigma S_\sigma^2$) results in smaller deviations from the d-orbital-only geometry in the four-coordinate complex

than in the three-coordinate one (Fig. 11). This behavior is certainly what would be expected under the scheme. As we go down the periodic table, however, the D_{3h} d^{10} structure is often found in distorted environments (*45*), e.g., in $(Ph_3P)_2AuCl$, where the M—Cl bond is long and the angle between the two M—P bonds has opened up from 120°. This incipient two coordination is expected when, as at the bottom of the periodic table, the $(n + 1)s/nd$ orbital separation is small. Similar effects are found in five-coordinate d^{10} systems (*46*).

Some interesting points emerge from the preceding discussion. The molecular geometry is dominated by σ effects (we have used only σ energies in this discussion). The d orbitals involved in σ interactions are always the higher energy ones because these orbitals are metal–ligand σ antibonding. Thus, only where there are holes in the higher-energy d orbitals will there be any large differential d-orbital stabilization energy for a distorted geometry compared to the ligand-ligand determined geometry. Thus with reference to the four-coordinate geometries of Figs. 7 and 8 for d^0, d^1, d^2, low-spin d^3 and d^4 configurations, $\sum(\sigma)$ has the same value $(8\beta_\sigma S_\sigma^2)$ for all three geometries—square planar, cis-divacant, and tetrahedral. The latter geometry, the one determined by ligand-ligand interactions is, therefore, the structure adopted. This feature then rationalizes the widespread observation that the first few d electrons have little effect on the geometry of the molecule. Thus $TiCl_4$ (d^0) and VCl_4 (d^1) are both tetrahedral, but note the much larger difference in structure between $ZnCl_4^{-2}$ (d^{10}) and $CuCl_4^{-2}$ (d^9).

Molecular orbital calculations support these ideas. Small distortions from the ligand-ligand determined geometry are often found when asymmetric electron-charge distributions are present in orbitals involving π interactions only. The second- and third-row hexafluorides MF_6 (M = Mo—Rh, W—Pt) are octahedral molecules, but, where holes in the π-orbital manifold exist, small vibronic effects are observed (*47*, *48*). This type of behavior has often been labeled the "dynamic" Jahn–Teller effect to distinguish it from the gross structural effects noted earlier. We believe that these sizably smaller effects reflect the relative importance of π interactions compared to σ interactions in determining the angular geometry. On our molecular model described in this paper, the reason for smaller π interactions compared with σ ones is the smaller value of π compared to σ overlap integrals. This discrepancy is magnified since, in the stabilization energy of Fig. 1, the overlap integral appears as the square.

The gross geometry is thus determined by the orbital occupation numbers of the three highest d orbitals. If these three orbitals are

symmetrically occupied (with orbital occupation numbers 000, 111, 222), then the d-electron distribution is spherically symmetrical and the d-orbital electron configuration will not exert any distorting effect on the symmetrical ligand–ligand determined structure. Only when the distribution of electrons in these three orbitals is nonspherically symmetrical does the molecule distort as we have seen in the foregoing.

These generalizations have led to a set of rules with which to predict the lowest-energy geometry of a complex (*24*):

1. Neglect any electrons in the lowest two d orbitals. The *angular* geometry is determined by the occupation numbers of the three highest energy orbitals.

2. If the occupation numbers are symmetrical (000, 111, 222) then the VSEPR geometry will be observed.

3. If a hole exists in the highest-energy orbital (220, 221, 210, 110), then the structure will be that of maximum overlap with the lobes of $d_{x^2-y^2}$.[9] (A structure intermediate between this geometry and the VSEPR one may be observed for 221.)

4. If two holes exist symmetrically in the two highest energy orbital (200, 211, 100), then the structure will be that based on the octahedron containing the maximum number of cis ligands. (A structure intermediate between this geometry and the VSEPR one may be observed for 211.)

Obviously for some excited-state configurations, not contained in the scheme, e.g., 121, we need to calculate and compare the relevant stabilization energies for the various extreme geometries.

How do these conclusions fit in with the Jahn-Teller (*49*) theorem telling us that molecules with orbitally degenerate electronic states distort to lose this degeneracy? Some of the distortions we have seen and rationalized are allowed under the Jahn-Teller scheme, but very importantly others are not (*50*). For example,

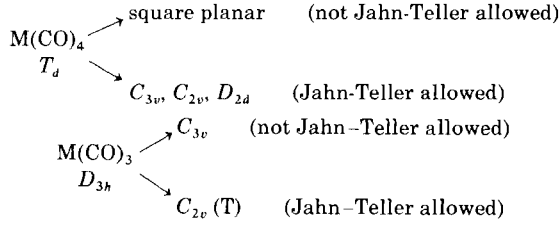

Thus, there is no reason from Jahn–Teller considerations considerations alone for $Fe(CO)_3$ (high-spin d^8) to distort from the D_{3h} geometry

[9] The first T-shaped geometry for a three coordinate is d^8 system has recently been found (*73*).

($^3A_2'$) to the observed C_{3v} structure ($^3A_2$), and the square planar structure for $Ni(CN_4)^{2-}$ is a very large distortion for a Jahn–Teller one. In fact, *all* the results of the "static Jahn–Teller" theorem are encompassed by the present theory, which is, as a consequence a much more powerful approach since it is able to provide energetic data on the geometry of any electronic configuration irrespective of any considerations concerning the degeneracy of the electronic state. On the present model, the smaller-energy changes involving the "dynamic Jahn–Teller" effect are considered to arise from the much smaller structural influence associated with asymmetrical charge distributions in π orbitals, as we have discussed in the preceding.

F. Derivation of Walsh Diagrams

The Walsh diagrams, showing qualitatively the energy changes associated with molecular orbitals on distortion, have a well-established place in main-group stereochemistry, but only recently have their equivalents in transition metal chemistry been comprehensively derived using the extended Hückel molecular orbital method (*13–16*). However, in some cases we may readily obtain the functional dependence on angle of distortion using the simple scheme developed here.

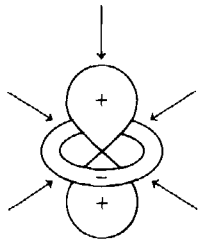

V

Consider the square pyramidal ML_5 unit with a geometry defined by the angle θ. Let us investigate how the stabilization energy associated with the d-orbital changes on distortion. d_{z^2} interacts with the axial ligand and the four equatorial ligands that overlap its collar (V). Thus, $\epsilon(d_{z^2}) = [1 + 4(1 - \frac{3}{2}\sin^2\theta)^2]\beta_\sigma S_\sigma^2$ from Table I; $d_{x^2-y^2}$ overlaps solely with the four equatorial ligands and hence $\epsilon(d_{x^2-y^2}) = 4(\sqrt{3}/2 \sin^2\theta)^2 S_\sigma^2$; d_{xz} and d_{yz}, which are σ nonbonding at $\theta = 90°$, give $\epsilon(d_{xz}, d_{yz}) = 4(\sqrt{3}/2 \sin 2\theta)^2 S_\sigma^2$. With these functions we can readily construct Fig. 12, where we see stabilization of d_{z^2} on bending away from 90°, but destabilization of d_{xz} and d_{yz}. Thus we find that whereas low-spin d^6 $Cr(CO)_6$ in a CH_4 matrix (*34a*) has a bond angle of 93°, low-spin d^7

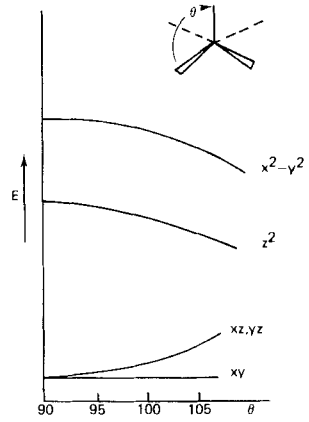

FIG. 12. Walsh diagram for distortion of a square pyramid.

$Co(CN)_5^{-3}$ has $\theta = 97°$ (*51*) and one-half of $Mn_2(CO)_{10}$ has $\theta = 96°$ (*52*). Similarly, high-spin Fe(II) in hemoglobin (*53*, *54*) lies 0.75 Å out of the plane of the porphyrin ring ($\theta > 90°$) but, in oxyhemoglobin (low-spin d^6), the iron now lies in the plane of the ring, $\theta \sim 90°$. The change in bond angle in the low-spin d^6, d^7 pair just mentioned is in the *opposite* direction to that expected if this "d electron" was stereochemically active in the sense of being one-half of a VSEPR electron pair (VI).

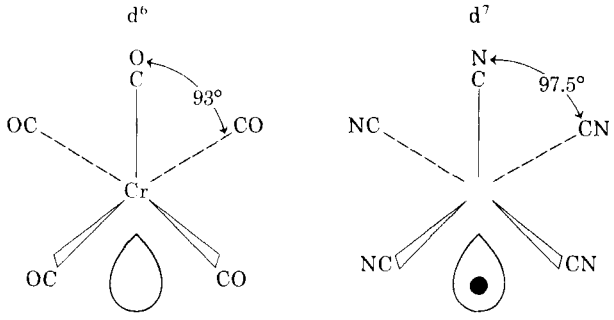

VI

G. Structural Consequences in d^8 and d^9 Systems

Three figures extracted from Tables III and IV and Fig. 5 are of immense importance in understanding some of the structural chemistry of low-spin d^8 and d^9 systems. We find that, for these two electronic configurations, the d-orbital stabilization energy of square planar, square pyramidal, and octahedral complexes are equal. This implies

that the axial bond energy between ligand σ and metal d orbitals in octahedral and square pyramidal low-spin d^8 and d^9 systems is zero and that the ligands are attached purely by forces involving the (s + p) orbital interactions on the metal.

Alternatively, we can see that the axial ligands (along the z axis) may only interact with d_{z^2}. The bonding orbital d_{z^2}–ligand is occupied but, in these d^8 and d^9 systems, also its antibonding counterpart contains two electrons resulting in a zero axial d-orbital–ligand bond order. Thus, we should expect to see, in general, long axial bond lengths compared to equatorial in these systems. Table VI shows some representative bond length data. For the six-coordinate d^9 case, we immediately recall that the Jahn–Teller theorem has been used for many years to rationalize these observations (*22*). It is easy to see, however, that the same distortion occurs irrespective of whether the parent compound is a six-coordinate regular octahedron (e.g., $CuCl_2$), a six-coordinate octahedron but with different ligands (e.g., $CuCl_2 \cdot 2H_2O$), or a five-coordinate square pyramid. Only the first case is directly approachable by Jahn–Teller considerations since only here are $d_{x^2-y^2}$ and d_{z^2} orbitals degenerate. Yet all three cases fit within the umbrella of the present discussion.

If a soft potential surface describes the approach of the axial ligand to the transition metal center, then it is not too surprising to see some short axial metal–ligand distances in a couple of instances (as in the example of K_2CuF_4 in Table VI) where possibly, because of crystal

TABLE VI

SOME BOND LENGTHS (Å) IN d^9 COMPLEXES

Octahedral:		
$CuCl_2$	4Cl at 2.30	2Cl at 2.95
$CsCuCl_3$	4Cl at 2.30	2Cl at 2.65
$CsCl_2 \cdot 2H_2O$	2O at 2.01	2Cl at 2.31
		2Cl at 2.98
$CuBr_2$	4Br at 2.40	2Br at 3.18
CuF_2	4F at 1.93	2F at 2.27
K_2CuF_4	2F at 1.95	4F at 2.08
Square pyramidal:		
Diquo(acac)Cu(II) picrate[a]	Equatorial 1.88; axial 2.76	
N,N'-disalicylidene ethylene diamine Cu(II)[b]	Equatorial 2.01; axial 2.41	

[a] D. Hall and T. N. Wates, *J. Chem. Soc.* p. 1644 (1960).

[b] R. D. Gillard and G. Wilkinson, *J. Chem. Soc.* p. 3599 (1963).

packing, the axial ligand may be pressed into the coordination shell. Under these circumstances, we see little change in the equatorial metal–ligand distances. In the recent crystal structure determination of $K_2PbCu(NO_2)_6$, there is even a regular octahedron of nitrogen atoms about the Cu^{2+} ion (*28c*). Often, because of this facile approach of the fifth and sixth ligands to the square plane, it is difficult to classify solid-state Cu(II) structures as four-, five-, or six-coordinate systems.

In d^8 chemistry the structural equivalent of this well-documented structural behavior is the so-called anomalous behavior of Ni(II) systems, in which two axial ligands may be weakly bound to a square planar unit (Lifschitz's salts) producing dramatic effects in the electronic spectrum (*55*). The d^8 system differs slightly from Cu(II) in the sense that the octahedral geometry has an additional stabilizing force. This is the exchange energy associated with the triplet state (high spin), which is obviously lower in energy than the singlet state (low spin) when $d_{x^2-y^2}$ and d_{z^2} are equienergetic. Sometimes the Lifschitz complexes [of Ni(II) with substituted ethylenediamines] are blue and paramagentic ("octahedral," high spin), and sometimes yellow and diamagnetic (square planar, low spin). The color depends on a variety of factors, such as the particular anions present, the solvent from which the material is crystallized, the temperature, and whether the complexes are exposed to atmospheric water vapor. In several cases, four-coordinate units polymerize to give Ni(II) in five- and six-coordinate environments, e.g., nickel acetylacetonate. The position of the equilibrium is generally complex and it is clear that low-energy pathways connect square planar four-, square pyramidal five-, and octahedral six-coordinate Ni(II).

The resemblance of the low-spin d^8 systems to the "Jahn–Teller" behavior in Cu(II) is forcefully apparent. Similarly, the X-ray crystal structure of square pyramidal (low-spin) $Ni(CN)_5^{-3}$ shows that the axial Ni—C bond length is much longer than the equatorial ones. In high-spin d^8 systems, since d_{z^2} and $d_{x^2-y^2}$ are now equally occupied, the d-orbital contributions to both sites should be equal, and in a large number of examples there is evidence to support this. In a recent comparison (*56a*) between the isostructural species $Mg(Me_3AsO)_5(ClO_4)_2$ (d^0) and $Ni(Me_3AsO)_5(ClO_4)_2$ (d^8), the axial MO bonds are 1.94 Å (Ni) and 1.92 Å (Mg) compared to the average equatorial bonds of 2.00 Å (Ni) and 2.03 Å (Mg). Compare these figures with those for low-spin $Ni(CN)_5^{-3}$ of 1.86 Å (equatorial) and 2.17 Å (axial) (*41a*). (In the latter molecule the axial bond length is certainly shortened to some extent by π bonding.)

Whereas the d-orbital stabilization energy difference between four and five coordination is zero for the low-spin d^8 configuration in the

electronic ground state, the same is not true if an excited-state configuration is produced with a different arrangement of d electrons, as in the high-spin d^8 complexes just discussed for example. This has led to the interesting and very unusual observation of photoassociation (*57*) in the molecule $Ir(MeNC)_4^+$. In the first excited state with configuration 211, there is a gain in d-orbital stabilization energy on adding a fifth ligand. The photo-produced complex dissociates in the dark.

H. Ligand Site Preferences

We may use the results of these last sections to inquire where in a mixed ML_nL_m' complex the strongest σ denors are likely to reside. In the low-spin d^8 square pyramid we saw in Section II, G that the axial bond was the weakest one. The isomer with the lowest energy will obviously be the one where the strongest σ donors (L) occupy those sites of largest latent bond strength. In the ML_4L' d^8 square pyramid, therefore, the weakest σ donor is relegated to the axial site.

Alternatively, we could have considered (*58*) that the most stable arrangement of the four remaining L ligands is the square planar structure, which is not disturbed by coordination of the fifth (weaker σ donor ligand). Quantitatively we may (*58*) use Eq. (9), define different values of $\beta_\sigma S_\sigma^2$ for each different ligand, and compare the stabilization energies for each isomer. All three approaches give us the same answer. For low-spin d^6 and high-spin d^8 systems, the stable four-coordinate geometry is the cis-divacant structure (VII). Thus the weaker σ donor here occupies an equatorial site in the square-based pyramid. However, Table III shows us that square planar and cis-divacant four-coordinate arrangements are very close in energy and, thus, the energy difference between the two isomers in these cases is small. Indeed, we see little difference in axial and equatorial bond lengths in a wide range of molecules with these electronic configurations surveyed by Orioli (*59*).

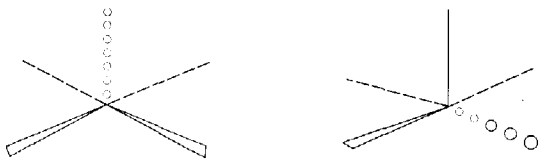

VII

For the d^8 low-spin trigonal bipyramid, we expect the stronger σ donors to occupy the axial positions from our preceding arguments. The T-shape three-coordinate structure (VIII) is much more stable

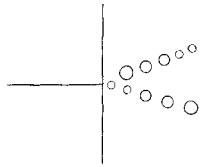

VIII

than the trigonal plane (Table V) for this electronic configuration. Alternatively, we may view the molecule in the following way (*60*). The total stabilization energy of the low-spin d^8 configuration arises from overlap (II) of ligand σ orbitals with d_{z^2}. (Fig. 8). Overlap of each axial ligand contributes $2\beta_\sigma S_\sigma^2$ to $\sum(\sigma)$ (from Table II), and each equatorial ligand $\frac{1}{2}\beta_\sigma S_\sigma^2$ since the latter overlap only with the collar of d_{z^2}. Thus, the axial positions contain the largest d-orbital stabilization, and it is here that the strongest σ donors should reside. With some exceptions, this is generally true. Shorter axial than equatorial bond lengths are found (Table VII) in all known low-spin d^8 trigonal bipyramidal complexes with first-row central atoms although the difference for $Fe(CO)_5$ is very small. [Recent reworking of the data suggests that there is no difference between the bond lengths of axial and equatorial groups within experimental error (*61*).] The situation is not quite as simple as we have suggested here, as evidenced by the disparity in bond lengths observed for $CdCl_5^{-3}$ and $HgCl_5^{-3}$ (d^{10})

TABLE VII

SOME BOND LENGTHS (Å) IN TRIGONAL BIPYRAMIDAL COMPLEXES

Complex	Axial	Equatorial	Ref.
$Ni(CN)_5^{-3}(d^8)$	1.838(9)	1.94[a]	41a
$Co(CNCH_3)_5^{+}(d^8)$	1.84(2)	1.88(2)	41c
$Fe(CO)_5(d^8)$	1.810(3)	1.833(2)	38
$CuCl_5^{-3}(d^9)$	2.2964(12)	2.3912(13)	41d
$CuBr_5^{-3}(d^9)$	2.4500(22)	2.5191(17)	41e
$CdCl_5^{-3}(d^{10})$	2.526(1)	2.561(2)	41f
$HgCl_5^{-3}(d^{10})$	2.518(4)	2.640(4)	46

[a] Average of several nonequivalent distances.

(Table VII). The tendency for the five-coordinate Hg complex to lose three ligands and become two-coordinate is reflected in the relative Hg—Cl bond lengths, and we have noted previously similar behavior in three-coordinate third-row d^{10} complexes. The usual explanation for this behavior [see Clegg (*45a*)] is the small d-s orbital separation at the bottom of the periodic table, i.e., heavy involvment of higher orbitals in determining the angular geometry. The trigonal bipyramidal $ZnCl_5^{-3}$ molecule is unfortunately unknown.

We may use similar arguments to conclude that six-coordinate octahedral low-spin d^6 ML_4L_2' are most stable in the cis configuration as is found to be largely the case, especially with first-row transition metals. Thus, *cis*-$Co(CN)_4(H_2O)_2^-$ is more stable (*62*) than the trans arrangement, although at 25°C in solution the two isomers are rapidly interconverting. The energy difference between them is probably small (cf. the d^6 square pyramid described in the foregoing). Similarly, for $M(CO)_4I_2$ (M = Fe, Ru, Os) the cis form is the more stable isomer (*63*). In a large number of FeL_4H_2 complexes (*64*) (L = phosphine, phosphite, CO), the cis form is of lower energy although the molecules are fluxional. For complexes with the large cage ligands P_4S_3, the cis forms are also the more stable (*65*) for $M(CO)_4(P_4S_3)_2$ (M = Cr, Mo). Here the trans isomer might be more likely on steric grounds. Similarly, the most stable ML_3L_3' species for low-spin d^6 should be the fac arrangement, which preserves the C_{3v} arrangement of strong-field ligands. Thus, $Co(CN)_3(H_2O)_3$ (*62*), $Cr(CO)_3(PH_3)_3$ (*66*), and $M(CO)_3(P_4S_3)_3$ (M = Cr, Mo) (*65*) are all found in this arrangement.

An interesting application of these ideas is the recent work on the rate of incorporation of ^{13}CO into $Mn(CO)_5Br$, $Re(CO)_5Br$, and $Cr(CO)_4$ chelate complexes (*67*). Thermally ^{13}CO is much more rapidly incorporated at the cis position of all three complexes than at the trans sites. By the microscopic reversibility principle, therefore, it is precisely at these sites where the ^{12}CO is preferentially labilized. We may view this in the following way. The lower energy of the two possible, square pyramidal intermediates in the case of $M(CO)_5Br$ will be the one that contains the cis-divacant arrangement of strong-field ligands as in $Cr(CO)_4$ itself. In these low-spin, d^6, five-coordinate fragments the weaker σ donor is, therefore, relegated to an equatorial position. Trans labilization, however, leaves behind a square planar strong-field ligand arrangement (IX), which is the less stable of the two. In the case of the tetracarbonyl chelate then, it is the "fac trivacant" structure which is the more stable tricarbonyl geometry (see the structure of $Cr(CO)_3$ noted above) and this is reached also by cis labilization from the six-coordinate structure.

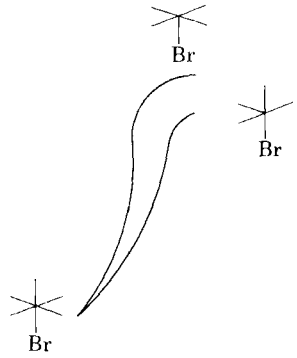

IX

I. Intramolecular Photochemical Rearrangements

The fact that the geometry of the transition metal complex depends on the precise arrangement of the electrons in the metal d orbitals means that in some cases the geometry and properties of an excited electronic state is different from that found for the electronic ground state. (We have already seen an interesting photoassociation reaction in Section II, G.) Thus, photochemical excitation is often sufficient to allow rearrangement processes to occur in otherwise stereochemically rigid systems. For example, the equilibrium geometry of the electronic ground state of the low-spin d^8 ML_2L_2' system is the square planar arrangement (cf. $Ni(CN)_4^{-2}$). The first excited state, however, with orbital occupation numbers (211) prefers the distorted tetrahedral arrangement typical of *high-spin* d^8 complexes. This rearrangement process in the excited state leads to facile (*68*) cis-trans photochemical isomerisation in solution:

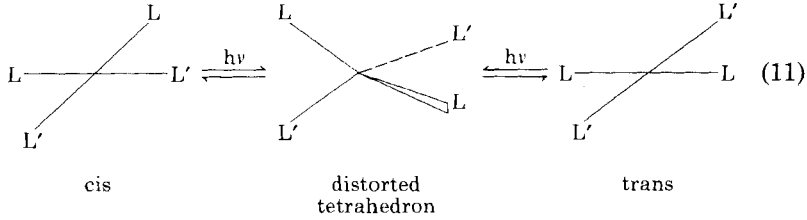

(11)

The ground-state interconversion via the distorted tetrahedron is prevented by a large barrier (see in the following). Similarly, although the electronic ground state of low-spin d^6 $Cr(CO)_5$ is square pyramidal (in the low-temperature matrix, any thermal fluxional behavior is frozen out), the geometry of the first excited state (intermediate-spin

d^6) is a trigonal bipyramid from Table IV. Thus, on photoexcitation, the square pyramid may rearrange via a process much akin to the Berry process proposed for $Fe(CO)_5$. There is an exchange of axial and basal ligands,

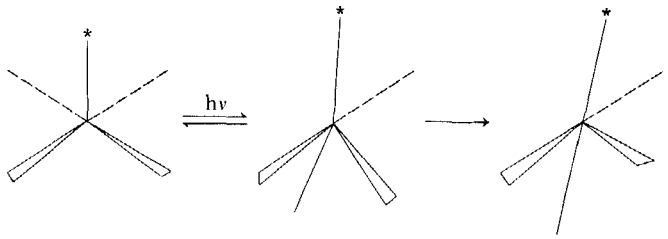

(12)

and this has been elegantly confirmed experimentally by the photochemical interconversion of the two isomers of $Cr(CO)_4CS$ in a low-temperature matrix (*69*).

The different spatial orientation of the right-hand product compared to starting material, indicated schematically in Eq. (12), has been followed (*70*) using polarized spectroscopy and photolysis for $Cr(CO)_5$ where there is no chemical "label" in the molecule. Both of these rearrangement processes are described by potential surfaces akin to the well-known cis ↔ trans ethylene interconversion (*71*). Figure 13 illustrates schematically for the square pyramidal/trigonal bipyramidal case an electronic ground state trapped in one of the two wells and

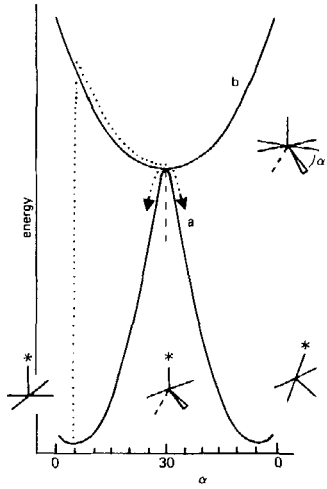

FIG. 13. Energy diagram showing interconversion of square pyramid and trigonal bipyramid for (a) d^6 low-spin ground state and (b) d^6 intermediate-spin excited state.

unable, because of the barrier between them, to interconvert thermally. These wells would equally well represent the square plane for Ni(II) L_2L_2'. The interconversion coordinate connecting the two wells is via the trigonal bipyramid (or distorted tetrahedron in the square planar examples). In the excited state, the equilibrium geometry is different from that in the ground state and the intramolecular rearrangement can proceed along the dotted pathway. (Some of the excited molecules will, of course, return to the original configuration.)

A third rearrangement process (*62*, *72*), that of cis → trans $Co(CN)_4(H_2O)_2^-$ and fac → mer $Co(CN)_3(H_2O)_3$ is also approachable (*58*) on the scheme. In the ground electronic state (low-spin d^6), as we have just noted, the cis and fac structures are more stable than their trans and mer analogs. In the first excited electronic state with orbital occupation numbers 210 or perhaps 110, the most stable geometry of the systems are the trans and mer isomers, however. On return to the electronic ground state, it is these geometries which are frozen out and slowly revert thermally to their more stable ground-state analogs.

III. Conclusion

We have seen that the d-orbital-only model of structural transition metal chemistry is remarkably successful in rationalizing a wide spectrum of observations from structural and kinetic transition metal chemistry. It is possibly even more remarkable because of the smaller contribution to the total stabilization energy (in the $M(H_2O)_6^{2+}$ series at least) of the n*d* orbitals compared to the $(n + 1)$s and $(n + 1)$p orbitals. Its validity we suspect will be better for first-row transition metal systems compared to complexes containing the heavier elements since, as we have noted herein, higher orbitals exert a significant distorting effect in Hg(II) and Au(I) chemistry. Although we should certainly consider the influence of these higher orbitals in any detailed discussion of these structural effects (see, for example, the finely worked reasoning in Ref. *14*), use of the d-orbital-only model provides a simple wide-ranging basic approach.

References

1. Sidgwick, N. V., and Powell, H. M., *Proc. Roy. Soc. London, Ser. A* **176**, 153 (1940).
2. (a) Gillespie, R. J., and Nyholm, R. S., *Q. Rev., Chem. Soc.* **11**, 339(1957); (b) Gillespie, R. J., *J. Chem. Educ.* **40**, 295 (1963); (c) *J. Chem. Soc.* pp. 4672, 4679 (1963); *Can. J. Chem.* **38**, 818 (1960); **39**, 318 (1961).
3. Gillespie, R. J., "Molecular Geometry." Van Nostrand-Rheinhold, London, 1972.
4. Walsh, A. D., *J. Chem. Soc.* pp. 2260, 2266, 2288, 2296, 2301 (1953).
5. (a) Gimarc, B. M., *J. Am. Chem. Soc.* **92**, 266 (1970); (b) **93**, 593 (1971); (c) **93**, 815 (1971).

6. Rauk, A., Allen, L. C., and Mislow, K., *J. Am. Chem. Soc.* **94**, 3035 (1972).
7. Gavin, R. M., *J. Chem. Educ.* **46**, 413 (1969).
8. Hoffmann, R., Howell, J. M., and Muetterties, E. L., *J. Am. Chem. Soc.* **94**, 3047 (1972).
9. (a) Bartell, L. S., *J. Chem. Educ.* **45**, 754 (1968); (b) Bartell, L. S., and Gavin, R. M., *J. Chem. Phys.* **48**, 2466 (1968).
10. (a) Pearson, R. G., *J. Am. Chem. Soc.* **91**, 4947 (1969); (b) *J. Chem. Phys.* **53**, 2986 (1970).
11. (a) Pearson, R. G., *J. Am. Chem. Soc.* **91**, 1252 (1969); (b) **94**, 8287 (1972); (c) *Acc. Chem. Res.* **4**, 152 (1971).
12. See, for example, Burdett, J. K., Dubost, H., Poliakoff, M., and Turner, J. J., *in* "Advances in Infra-red and Raman Spectroscopy" (R. J. H. Clark and R. E. Hester, eds.) Vol. 11, Heyden, London, 1976.
13. Burdett, J. K., *J. Chem. Soc., Faraday 2* **70**, 1599 (1974).
14. (a) Elian, M., and Hoffmann, R., *Inorg. Chem.* **14**, 1058 (1975); (b) Rossi, A. R., and Hoffmann, R., *ibid.* **14**, 305 (1975).
15. Rosch, N., and Hoffmann, R., *Inorg. Chem.* **13**, 2656 (1974).
16. (a) Hoffmann, R., Chen, M. L., Elian, M., Rossi, A. R., and Mingos, D. M. P., *Inorg. Chem.* **13**, 2666 (1974); (b) Enemark, J. H., and Feltham, R. D., *J. Am. Chem. Soc.* **96**, 5003, 5004 (1974).
17. (a) Schaffer, C. E., *Struct. Bonding (Berlin)* **14**, 69 (1973); (b) *Proc. Roy. Soc., London A* **297**, 96 (1967); (c) Schaffer, C. E., and Jorgensen, C. K., *Mol. Phys.* **9**, 401 (1965); (d) Schaffer, C. E., *Pure Appl. Chem.* **24**, 361 (1970); (e) Gerloch, M., and Slade, R. C., "Ligand Field Parameters." Cambridge Univ. Press, London and New York, 1973; (f) Kettle, S. F. A., *J. Chem. Soc. A* 420 (1966); (g) Larsen, E., and La Mar, G. N., *J. Chem. Educ.* **51**, 633 (1974); (h) For application of the angular overlap model to main group stereochemistry, see Burdett, J. K., *Struct. Bonding (Berlin)* **31**, 67 (1976).
18. Bartell, L. S., and Plato, V., *J. Am. Chem. Soc.* **95**, 3097 (1973).
19. McClure, D. S., *in* "Advances in the Chemistry of the Coordination Compounds" (S. Kirschner, ed.) Macmillan, New York, 1961.
20. Smith, W., and Clack, D., *Rev. Roum. Chim.* **20**, 1243 (1975).
21. Burdett, J. K., *J. Chem. Soc., Dalton Trans.*, p. 1725 (1976).
22. See, for example, Cotton, F. A., and Wilkinson, G., *in* "Advanced Inorganic Chemistry." Wiley, New York, 1972.
23. Cotton, F. A., *J. Chem. Educ.* **41**, 466 (1964).
24. Burdett, J. K., *Inorg. Chem.* **14**, 375 (1975).
25. Eigen, M., *Pure Appl. Chem.* **6**, 105 (1963).
26. See also Bennett, H. D., and Caldin, B. F., *J. Chem. Soc. A* p. 2198 (1971).
27. Philipps, C. S. G., and Williams, R. J. P. "Inorganic Chemistry" Oxford Univ. Press, London and New York, 1966.
28. (a) Willett, R. D., *J. Chem. Phys.* **41**, 2243 (1964); (b) Morosin, B., and Lingafelter, *Acta Crystallogr.* **13**, 807 (1960); (c) Issacs, N. W., Kennard, C. H. L., and Wheeler, D. A., *J. Chem. Soc.A* 386 (1969).
29. (a) Willett, R. D., Ferraro, J. R., and Choca, M., *Inorg. Chem.* **13**, 2919 (1974); (b) Wang, P. J., and Drickamer, H. G., *J. Chem. Phys.* **59**, 559 (1973).
30. Ferraro, J. R., and Long, J., *Acc. Chem. Res.* **8**, 171 (1975).
31. (a) Crichton, O., Poliakoff, M., Rest, A. J., and Turner, J. J., *J. Chem. Soc., Dalton Trans.* p. 1321 (1975); (b) Ozin, G. A., *in* "Vibrational Spectroscopy of Trapped Species" (H. E. Hallam, ed.), Wiley, New York, 1973; (c) Huber, H., Hanlan, L., McGarvey, B., Kundig, E. P., and Ozin, G. A., *J. Am. Chem. Soc.* **97**, 7054 (1975).

32. Perutz, R. N., and Turner, J. J., *J. Am. Chem. Soc.* **97**, 4800 (1975).

33. (a) Poliakoff, M., and Turner, J. J., *J. Chem. Soc.* 1351 (1973); (b) 2276 (1974).

34. (a) Perutz, R. N., and Turner, J. J., *Inorg. Chem.* **14**, 262 (1965); (b) Burdett, J. K., Graham, M. A., Perutz, R. N., Poliakoff, M., Rest, A. J., Turner, J. J., and Turner, R. F., *J. Am. Chem. Soc.* **97**, 4805 (1975); (c) A trigonal bipyramidal geometry was incorrectly assigned by Kundig, E. P., and Ozin, G. A., *ibid.* **96**, 3820 (1974); (d) Perutz, R. N., and Turner, J. J., *ibid.* **97**, 4791 (1975); (e) Graham, M. A., Poliakoff, M., and Turner, J. J., *J. Chem. Soc. A* p. 2939 (1971).

35. Huber, H., Kundig, E. P., and Ozin, G. A., *J. Am. Chem. Soc.* **96**, 5585 (1974).

36. Huber, H., Kundig, E. P., Ozin, G. A., and Poe, A. J., *J. Am. Chem. Soc.* **97**, 308 (1975).

37. Veillard, A., private communication.

38. Beagley, B., Cruickshank, D. W. J., Pinder, P. M., Robiette, A. G., and Sheldrick, G. M., *Acta Crystallogr., Sect. B* **25**, 737 (1969).

39. Frenz, B. A., and Ibers, J. A., *Inorg. Chem.* **11**, 1109 (1972).

40. Berry, R. S., *J. Chem. Phys.* **32**, 933 (1960).

41. (a) Raymond, K. N., Corfield, D. W. R., and Ibers, J. A., *Inorg. Chem.* **7**, 1362 (1968); (b) Basile, L. J., Ferraro, J. R., Choca, M., and Nakamoto, K., *ibid.* **13**, 496 (1974); (c) Cotton, F. A., Dunne, T. G., and Wood, J. S., *ibid.* **4**, 318 (1965); (d) Raymond, K. N., Meek, D. W., and Ibers, J. A., *ibid.* **7**, 1111 (1968); (e) Goldfield, S. A., and Raymond, K. N., *ibid.* **10**, 2604 (1971); (f) Long, T. V., Herlinger, A. W., Epstein, E. F., and Bernal, I., *ibid.* **9**, 459 (1970).

42. Burdett, J. K., and Turner, J. J., *in* "Cryogenic Chemistry" (G. A. Ozin and M. Moskovits, eds.) Wiley, New York, 1976.

43. (a) Dekock, R. L., *Inorg. Chem.* **10**, 1205 (1971); (b) Kundig, E. P., Moskovits, M., and Ozin, G. A., *Can. J. Chem.* **51**, 2710 (1975); (c) Huber, H., Kundig, E. P., Moskovits, M., and Ozin, G. A., *J. Am. Chem. Soc.*, **95**, 332 (1973); (d) Kundig, E. P., Moskovits, M., and Ozin, G. A., *J. Mol. Struct.* **14**, 137 (1972).

44. Poliakoff, M., *J. Chem. Soc., Dalton Trans.* 210 (1974).

45. (a) Clegg, W., *Acta Crystallogr., Sect. B* **32**, 2712 (1976); (b) Guggenberger, L. J., *J. Organomet. Chem.* **81**, 271 (1974); (c) Baenziger, N. C., Dittemore, K. M., and Doyle, J. R., *Inorg. Chem.* **13**, 805 (1974); (d) Wijhoven, J. G., Bosman, W. P. J. H., and Beurskens, P. T., *J. Cryst. Mol. Struct.* **2**, 7 (1972); (e) Canty, A. J., Marker, A., and Gatehouse, B. M., *J. Organomet. Chem.* **88**, C31 (1975).

46. Clegg, W., Greenhalgh, D. A., and Straughan, B. P., *J. Chem. Soc., Dalton Trans.* 2591 (1975).

47. (a) Seip, H. M., and Seip, R., *Acta Chem. Scand.* **20**, 2698 (1966); (b) Kimura, M., Schomaker, V., Smith, D. W., and Weinstock, B., *J. Chem. Phys.* **48**, 4001 (1968); (c) Jacob, E. J., and Bartell, L. S., *ibid.* **53**, 2231 (1970).

48. Weinstock, B., and Goodman, G. L., *Advan. Chem. Phys.* **9**, 169 (1966).

49. Jahn, H. A., and Teller, E., *Proc. Roy. Soc., London, Ser. A* **161**, 220 (1937).

50. Jotham, R. W., and Kettle, S. F. A., *Inorg. Chim. Acta* **5**, 183 (1971).

51. Brown, L. D., and Raymond, K. N., *J. Chem. Soc., Chem. Commun.* **910** (1974).

52. Bennett, M., and Mason, R., *Nature (London)* **205**, 760 (1965).

53. (a) Perutz, M. F., *Nature (London)* **228**, 726 (1970); (b) **237**, 495 (1972).

54. Williams, R. J. P., *in* "Iron in Biochemistry and Medicine" (A. Jacobs and M. Worwood, eds.) Academic Press, New York, 1974.

55. (a) Higginson, W. C. E., Nyburg, S. C., and Wood, J. S., *Inorg. Chem.* **3**, 463 (1964); (b) Nyburg, S. C., and Wood, J. S., *ibid.* **3**, 468 (1964).

56. (a) Ng, Y. S., Rodley, G. A., and Robinson, W. T., *Inorg. Chem.* **15**, 303 (1976); (h) Sacconi, L., *Coord. Chem. Rev.* **8**, 351 (1972).

57. Bedford, W. M., and Rouchias, G., *J. Chem. Soc., Chem. Commun.* p. 1224 (1972).

58. Burdett, J. K., *Inorg. Chem.* **15**, 212 (1976).
59. Orioli, P. L., *Coord. Chem. Rev.* **6**, 285 (1971).
60. Burdett, J. K., *Inorg. Chem.* **14**, 931 (1975).
61. Robiette, A. G., private communication (1976).
62. (a) Viane, L., D'Olieslager, J., and De Jaegere, S., *Inorg. Chem.* **14**, 2736 (1975); (b) *J. Inorg. Nucl. Chem.* **37**, 2435 (1975).
63. (a) Pankowski, M., and Bigorgne, M., *J. Organomet. Chem.* **19**, 393 (1969); (b) Johnson, B. F. G., Lewis, J., Robinson, D. W., and Miller, R., *J. Chem. Soc. A* p. 1043 (1968).
64. Muetterties, E. L., *Acc. Chem. Res.* **3**, 266 (1970).
65. Jefferson, R., Klein, H. F., and Nixon, J. F., *J. Chem. Soc., Chem. Commun.* p. 536 (1969).
66. Fischer, E. O., Louis, E., and Kreiter, C. G., *Angew. Chem., Int. Ed. Engl.* **8**, 377 (1969).
67. (a) Attwood, J. D., and Brown, T. L., *J. Am. Chem. Soc.* **97**, 3380 (1975); (b) **98**, 3155, 3160 (1976); (c) Cohen, M. A., and Brown, T. L., *Inorg. Chem.* **15**, 1417 (1976).
68. (a) Haake, P., and Hylton, T. A., *J. Am. Chem. Soc.* **84**, 3774 (1962); (b) Balzani, V., Carassiti, V., Moggi, L., and Scandola, F., *Inorg. Chem.* **4**, 1243 (1965); (c) McGarvey, J. J., and Wilson, J., *J. Am. Chem. Soc.* **97**, 2531 (1975); (d) Eaton, D. R., *ibid.* **90**, 4272 (1968); (e) Whitesides, T. H., *ibid.* **91**, 2395 (1969).
69. Poliakoff, M., *Inorg. Chem.* **15**, 2022, 2892 (1976).
70. (a) Burdett, J. K., Perutz, R. N., Poliakoff, M., and Turner, J. J., *J. Chem. Soc., Chem. Commun.* p. 157 (1975). (b) Burdett, J. K., Gryzbowski, J. M., Perutz, R. N., Poliakoff, M., Turner, J. J., and Turner, R. F., *Inorg. Chem.* **17**, 147 (1978).
71. Salem, L., and Stohrer, W. D., *J. Chem. Soc., Chem. Commun.* p. 140 (1975).
72. Viane, L., D'Olieslager, J., and De Jaegere, S., (unpublished results).
73. Yared, Y. W., Miles, S. L., Bav, R., and Reed, C. A., *J. Am. Chem. Soc.* **99**, 7076 (1977).